JOURNAL OF Materials CHEMISTRY

Magnetic and calorimetric studies on $Ba_3LnRu_2O_9$ (Ln = Gd, Ho–Yb) with 6H-perovskite structure

Yoshihiro Doi and Yukio Hinatsu

Division of Chemistry, Graduate School of Science Hokkaido University, Sapporo 060-0810, Japan

Received 17th December 2001, Accepted 19th March 2002
First published as an Advance Article on the web 15th April 2002

Crystal structures and magnetic properties of the quaternary oxides $Ba_3LnRu_2O_9$ (Ln = Gd, Ho–Yb) are reported. These compounds have the 6H-perovskite structure with space group $P6_3/mmc$. This structure consists of linkages between LnO_6 octahedra and Ru_2O_9 dimers made from face-shared RuO_6 octahedra. From their magnetic susceptibility and specific heat measurements, we have found that these compounds show magnetic anomalies at 14.8 K (Ln = Gd), 10.2 K (Ho), 6.0 K (Er), 8.3 K (Tm), and 4.5 K (Yb). It is considered that they are due to the antiferromagnetic interaction between Ln^{3+} ions.

Introduction

The perovskite and perovskite-like oxides containing ruthenium ions show a variety of electronic properties and have attracted a great deal of interest.[1,2] Recently, the crystal structures and magnetic properties of the ordered perovskites A_2LnRuO_6 (A = Sr or Ba; Ln = lanthanide elements) have been investigated. For example, Sr_2LnRuO_6 compounds (Ln = Eu–Lu) exhibit an antiferromagnetic transition at 30–46 K and they show a complex temperature dependence of their magnetic susceptibilities below these temperatures.[3] In many cases, these magnetic transitions may be due to the magnetic interaction between the Ru^{5+} ([Kr]$4d^3$ electronic structure; [Kr] = krypton core) and Ln^{3+} ([Xe]$4f^n$ electronic structure; [Xe] = xenon core) ions, which is *via* a superexchange pathway of Ru–O–Ln.

We turn our attention to the magnetic properties of the ternary oxides $Ba_3LnRu_2O_9$ with the 6H-$BaTiO_3$-type structure.[4] In these compounds, Ru and Ln ions occupy the face-sharing octahedral sites (Ru_2O_9 dimer) and the corner-sharing octahedral ones (LnO_6 octahedron), respectively. The predicted superexchange pathways are Ru–O–Ru and Ru–O–Ln. The magnetic coupling between Ru ions in the former pathway is usually antiferromagnetic and strong because the distance between two Ru ions is very short ($\sim$2.5 Å). The latter pathway resembles the pathway found in the ordered perovskites A_2LnRuO_6. Thus, it is expected that various magnetic cooperative phenomena due to the interactions between d and f electrons will be observed at low temperatures. In our earlier work, we found that $Ba_3NdRu_2O_9$ shows a crystal phase transition at *ca.* 120 K and a ferromagnetic transition of Nd^{3+} ions at 24 K.[5] In addition, $Ba_3PrRu_2O_9$ and $Ba_3TbRu_2O_9$ show antiferromagnetic transitions at 10.5 K and 9.5 K, respectively.[6]

In this paper, we report the crystal structure and magnetic properties of $Ba_3LnRu_2O_9$ with heavy lanthanide elements, *i.e.*, Ln = Gd, Ho–Yb, through their X-ray diffraction, magnetic susceptibility, and specific heat measurements.

Experimental

Polycrystalline samples of $Ba_3LnRu_2O_9$ (Ln = Gd, Ho–Yb) were synthesized by a solid-state reaction. Powders of barium carbonate ($BaCO_3$), ruthenium oxide (RuO_2), and lanthanide oxides (Ln_2O_3), each material with a purity of more than 99.9%, were used as starting materials. They were weighed in an appropriate metal ratio and well mixed in an agate mortar. The mixtures were pressed into pellets and then calcined at 900 °C for 12 hours. The calcined materials were initially fired in air at 1200 °C for 12 × 2 hours, and were fired at 1300 °C for 12 × 5 hours with several intermediate grindings and pelletings.

Powder X-ray diffraction profiles for all samples were measured in the range $10° \leqslant 2\theta \leqslant 120°$ using Cu-Kα radiation on a Rigaku MultiFlex diffractometer. Crystal structures were determined by the Rietveld technique, using the program RIETAN2000.[7]

CCDC reference numbers 179191–179195. See http://www.rsc.org/suppdata/jm/b1/b111504a/ for crystallographic data in CIF or other electronic format.

Magnetic susceptibility measurements were carried out using a SQUID magnetometer (Quantum Design, MPMS-5S). The temperature dependence of the magnetic susceptibilities was measured under both zero-field-cooled (ZFC) and field-cooled (FC) conditions in an applied field of 0.1 T over the temperature range 1.8–400 K.

Specific heat measurements were performed using a relaxation technique with a commercial heat capacity measurement system (Quantum Design, PPMS model) in the temperature range 1.8–300 K. The sintered sample in the form of a pellet was mounted on a thin alumina plate with grease for better thermal contact.

Results and discussion

Crystal structures

The results of the X-ray diffraction measurements show that $Ba_3LnRu_2O_9$ (Ln = Gd, Ho–Yb) are formed as single-phase materials. Fig. 1 shows the diffraction pattern for $Ba_3HoRu_2O_9$, as an example. Their X-ray diffraction profiles were indexed on hexagonal cells with the space group $P6_3/mmc$ (No. 194), and their crystallographic parameters were analyzed by the Rietveld technique. The schematic structure of $Ba_3LnRu_2O_9$ is illustrated in Fig. 2. This crystal structure has two octahedral sites: the face-sharing octahedral site occupied by Ru ions (Ru_2O_9 dimer) and the corner-sharing octahedral site occupied by Ln ions (LnO_6 octahedron). Neither the cation disorder between these two sites nor oxygen defect were found within the error of these analyses. This crystal structure agrees with those for other $Ba_3LnRu_2O_9$ compounds reported previously.[5,8–10]

The crystallographic parameters and reliability factors are

 DOI: 10.1039/b111504a

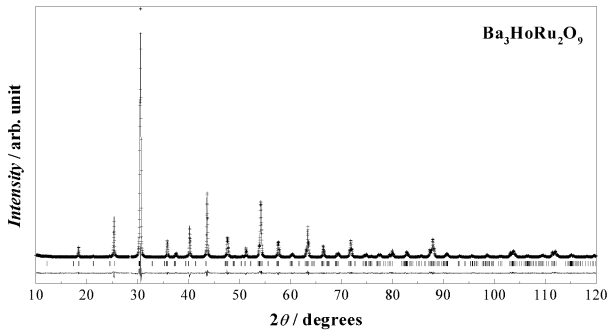

Fig. 1 X-Ray diffraction profile for $Ba_3HoRu_2O_9$. The calculated and observed profiles are shown on the top as a solid line and cross markers, respectively. The vertical marks show positions calculated from Bragg reflections. The bottom trace is a plot of the difference between the calculated and observed intensities.

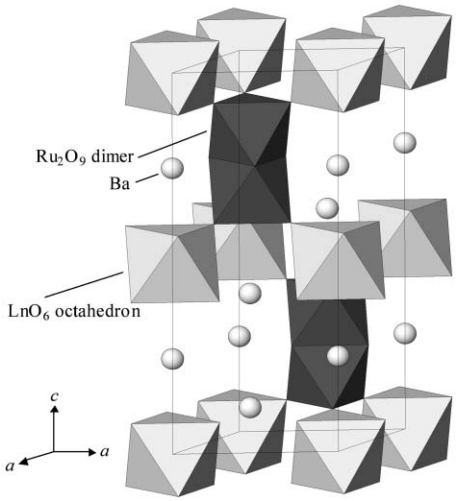

Fig. 2 The schematic structure of $Ba_3LnRu_2O_9$.

summarized in Table 1. Some selected bond lengths and angles are listed in Table 2. The lattice parameters and the Ln–O bond lengths increase monotonously with the size of the Ln^{3+} ion.

Table 1 Structural parameters for $Ba_3LnRu_2O_9$

	Gd	Ho	Er	Tm	Yb
a/Å	5.9097(2)	5.8838(2)	5.8764(2)	5.8686(2)	5.8616(2)
c/Å	14.6101(3)	14.5064(5)	14.4794(4)	14.4537(5)	14.4321(4)
Ba1 *B*/Å^2	0.42(5)	0.74(3)	0.67(2)	0.23(3)	0.29(4)
Ba2 *z*	0.9040(1)	0.9063(1)	0.9068(1)	0.9072(1)	0.9076(1)
Ba2 *B*/Å^2	0.88(3)	0.74	0.67	0.23	0.86(3)
Ln *B*/Å^2	0.23(5)	0.10(5)	0.10(4)	0.20(4)	0.33(4)
Ru *z*	0.1635(1)	0.1622(1)	0.1621(1)	0.1620(1)	0.1618(1)
Ru *B*/Å^2	0.18(3)	0.18(3)	0.10(3)	0.20(4)	0.15(3)
O1 *x*	0.4891(7)	0.4884(7)	0.4876(7)	0.4882(7)	0.4875(7)
O1 *B*/Å^2	0.9(2)	0.9(1)	0.8(1)	0.7(1)	0.6(2)
O2 *x*	0.1772(6)	0.1758(7)	0.1754(5)	0.1751(5)	0.1748(5)
O2 *z*	0.4105(4)	0.4125(4)	0.4127(4)	0.4125(4)	0.4124(4)
O2 *B*/Å^2	1.1(2)	0.9	0.8	0.7	1.2(2)
R_{wp} (%)	11.75	11.98	10.83	10.78	11.25
R_I (%)	2.00	2.58	2.04	2.35	1.76
R_F (%)	1.39	1.65	1.27	1.63	1.09
R_e (%)	8.42	8.69	7.58	8.10	7.64

[a]Space group: $P6_3/mmc$; $Z = 2$. Atomic positions: Ba(1) 2*b*(0,0,1/4); Ba(2) 4*f*(1/3,2/3,*z*); Ln 2*a*(0,0,0); Ru 4*f*(1/3,2/3,*z*); O(1) 6*h*(*x*,2*x*,1/4); O(2) 12*k*(*x*,2*x*,*z*). [b]Definitions of reliability factors R_{wp}, R_I, R_F and R_e are given as follows: $R_{wp} = [\Sigma w(|F_o| - |F_c|)^2/\Sigma w|F_o|^2]^{1/2}$, $R_I = \Sigma|I_{ko} - I_{kc}|/|I_{kc}|/I_{kc}|/\Sigma I_{ko}$, $R_F = \Sigma|I_{ko}{}^{1/2} - I_{kc}{}^{1/2}|/\Sigma I_{ko}{}^{1/2}$, $R_e = [(N-p)/\sum_i w_i y_i^2]^{1/2}$.

Table 2 Selected bond lengths (Å) and angles (°) for $Ba_3LnRu_2O_9$

	Gd	Ho	Er	Tm	Yb
Ba(1)–O(1)	2.957(1)	2.944(1)	2.941(1)	2.937(1)	2.934(1)
Ba(1)–O(2)	2.964(6)	2.960(7)	2.956(6)	2.947(6)	2.940(6)
Ba(2)–O(1)	2.893(5)	2.905(5)	2.911(4)	2.907(5)	2.912(4)
Ba(2)–O(2)	2.958(1)	2.944(1)	2.941(1)	2.936(1)	2.933(1)
Ba(2)–O(2)	3.147(6)	3.081(7)	3.068(6)	3.063(6)	3.056(6)
Ru–O(1)	2.034(6)	2.029(6)	2.021(5)	2.024(6)	2.018(5)
Ru–O(2)	1.929(6)	1.937(6)	1.938(5)	1.935(6)	1.933(5)
Ru–O (average)	**1.982(6)**	**1.983(6)**	**1.980(5)**	**1.980(6)**	**1.976(5)**
Ru–Ru	**2.527(3)**	**2.547(3)**	**2.545(3)**	**2.543(3)**	**2.547(3)**
Ln–O(2)	2.237(6)	2.196 (7)	2.188(5)	2.184(6)	2.178(5)
Ru–O(2)–Ln	178.3(3)	178.7(4)	178.7(3)	178.4(3)	178.2(3)
Ru–O(1)–Ru	76.8(3)	77.7(3)	78.0(3)	77.9(3)	78.3(3)

The Ru–O(1) and Ru–O(2) bond lengths are 2.018–2.029 Å and 1.921–1.939 Å, respectively, indicating that two octahedra in this Ru_2O_9 dimer are distorted in shape.

The average Ru–O bond lengths are 1.974–1.983 Å, the value of which is in the middle between 1.989–1.997 Å for the $Ru^{4+}{}_2O_9$ dimer of $Ba_3LnRu_2O_9$ (Ln = Ce, Pr, Tb)[6] and 1.965 Å for the $Ru^{5+}{}_2O_9$ dimer of $Ba_3MRu_2O_9$ (M = Zn and Ni).[11] This result indicates that the average valency of Ru ions is +4.5. The interatomic distance between two ruthenium ions (Ru–Ru) in the Ru_2O_9 dimer is in the range 2.527–2.547 Å, which is longer than that in the $Ru^{4+}{}_2O_9$ dimer (2.481–2.493 Å[6,10]) and shorter than that in the $Ru^{5+}{}_2O_9$ dimer (2.681–2.685 Å[5,9,10]). This tendency may be explained by the difference in the strength of the electrostatic repulsion between ruthenium, *i.e.*, the Ru–Ru distance becomes larger with increasing the average valence of ruthenium ions. Therefore, these relations are also consistent with the above discussion that the average valency of Ru ions is +4.5.

Magnetic susceptibilities

The temperature dependence of reciprocal magnetic susceptibilities for $Ba_3LnRu_2O_9$ (Ln = Gd, Ho–Yb) is shown in Fig. 3. The susceptibility data in the higher temperature region ($T > 150$ K) are fitted with the Curie–Weiss law; the effective magnetic moments μ_{eff} and Weiss constants θ are listed in Table 3. The Weiss constants are negative; therefore, the predominant magnetic interactions in these compounds are antiferromagnetic. The effective magnetic moments are obviously close to those for the free Ln^{3+} ions ($\mu_{Ln^{3+}}$) rather

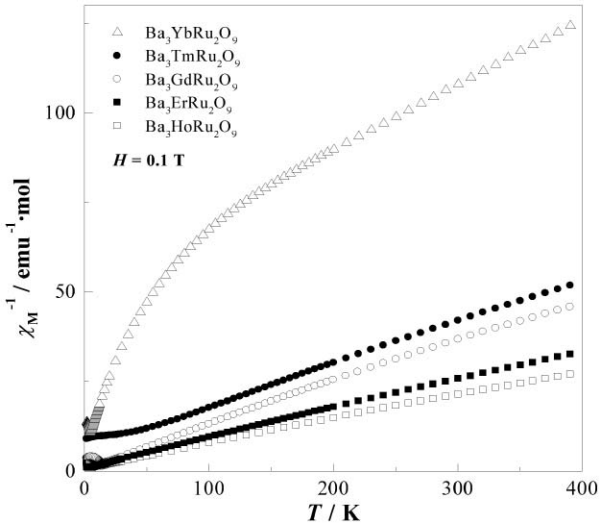

Fig. 3 Temperature dependence of reciprocal magnetic susceptibilities for $Ba_3LnRu_2O_9$.

Table 3 The magnetic moments for free Ln^{3+} ion (μ_{Ln3+}), calculated magnetic moments for all ions (μ_{cal}), effective magnetic moments (μ_{eff}) and Weiss constants (θ) for $Ba_3LnRu_2O_9$ (Gd, Ho–Yb)

Ln^{3+}	$\mu_{Ln^{3+}}/\mu_B$	μ_{cal}/μ_B	μ_{eff}/μ_B	θ/K
Gd^{3+}	7.94	9.28	7.68(1)	−2.9(5)
Ho^{3+}	10.58	11.62	10.15(1)	−5.4(4)
Er^{3+}	9.59	10.72	9.45(2)	−9.9(7)
Tm^{3+}	7.55	8.94	7.35(1)	−24.5(5)
Yb^{3+}	4.54	6.60	5.26(1)	−178(2)

[a]Note: $\mu_{cal} = \sqrt{\mu_{Ln^{3+}}{}^2 + \mu_{Ru^{4+}(lowspin)}{}^2 + \mu_{Ru^{5+}}{}^2}$

than the values calculated from

$$\mu_{cal} = \sqrt{\mu_{Ln^{3+}}{}^2 + \mu_{Ru^{4+}}{}^2 + \mu_{Ru^{5+}}{}^2}$$

This fact indicates that the contribution of Ru ions to the effective magnetic moment is very small. Therefore, the Ru ions should no longer be in the paramagnetic state in this temperature range; the magnetic moments of two Ru ions in each Ru_2O_9 dimer are coupled antiferromagnetically. Similar antiferromagnetic coupling was reported in the analogous 6H-perovskites $Ba_3M^{2+}Ru^{5+}{}_2O_9$ (M = Mg, Ca, Cd, and Sr).[12,13]

Figs. 4–8(a) show the temperature dependence of the magnetic susceptibility for each compound at low temperatures. It is found that $Ba_3LnRu_2O_9$ show magnetic anomalies at 14.8 K (Ln = Gd), 10.2 K (Ho), 6.0 K (Er), 8.3 K (Tm), and 4.5 K (Yb). In order to clarify these magnetic anomalies, we performed specific heat measurements.

Specific heats

Figs. 4–8(b) show the variation of the specific heats (C_p) as a function of temperature. The specific heat of any compound shows a λ-type anomaly at the same temperature at which the magnetic anomaly is observed in the susceptibility *vs.* temperature curve. This result indicates that these anomalies are an antiferromagnetic transition.

The specific heat mainly consists of the lattice, electronic, and magnetic specific heats. In order to estimate the lattice and electronic contributions, we used a polynomial function of the temperature, $f(T) = aT^3 + bT^5 + cT^7$, in which the constants were determined by fitting this function to the observed specific heat data between 20 and 40 K. Each calculated curve is shown in Figs. 4–8(b) as a dotted curve. The magnetic specific heat

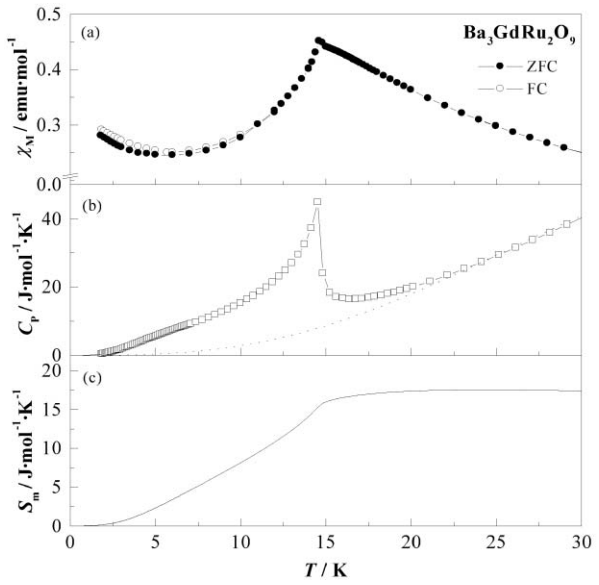

Fig. 4 Temperature dependence of (a) the magnetic susceptibility, (b) the specific heat and (c) the magnetic entropy of $Ba_3GdRu_2O_9$.

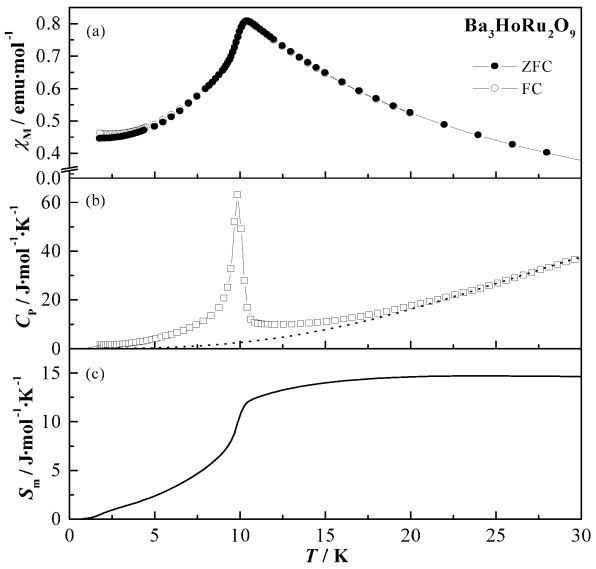

Fig. 5 Temperature dependence of (a) the magnetic susceptibility, (b) the specific heat and (c) the magnetic entropy of $Ba_3HoRu_2O_9$.

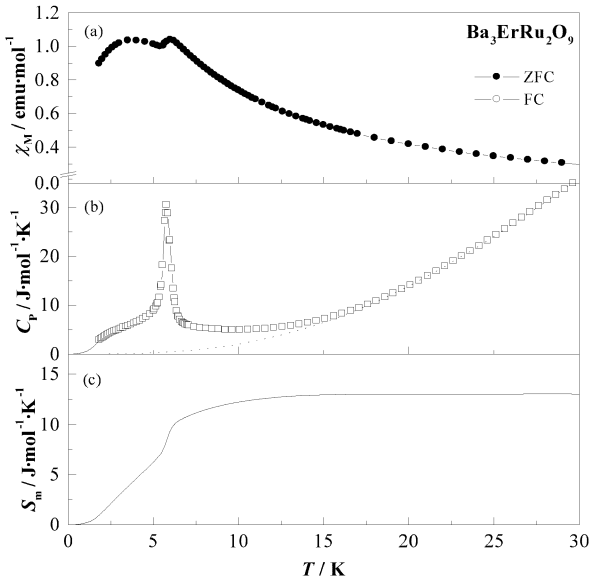

Fig. 6 Temperature dependence of (a) the magnetic susceptibility, (b) the specific heat and (c) the magnetic entropy of $Ba_3ErRu_2O_9$.

(C_m) for $Ba_3LnRu_2O_9$ is obtained by subtracting the lattice and electronic contributions from the total specific heat, *i.e.*, $C_m(T) = C_p(T) - f(T)$.

The temperature dependence of the magnetic entropy calculated by $S_m = \int \frac{C_m}{T} dT$ is shown in Figs. 4–8(c). As will be described later, the magnetic transitions observed for these $Ba_3LnRu_2O_9$ compounds are due to the magnetic ordering of Ln^{3+} ions, because the estimated magnetic entropy changes are large enough for the Ln^{3+} ordering. In addition, there may be a contribution of the magnetic interaction between antiferromagnetically coupled $Ru^{4.5+}{}_2O_9$ dimers, which have one unpaired electron per dimer at sufficiently low temperatures, to the magnetic entropy change. We have already measured the magnetic susceptibility and specific heat for $Ba_3M^{3+}Ru^{4.5+}{}_2O_9$ (M = Y, In, La and Lu) in which only Ru ions are magnetic. They show antiferromagnetic transitions at about 4.5 K (for Ln = Y and In), 6.0 K (La), and 9.5 K (Lu), and the magnetic entropy change for such magnetic transitions is about 3 J mol^{-1} K^{-1} (Y, In, Lu) and 0.3 J mol^{-1} K^{-1} (La).[14]

The magnetic entropy change associated with the antiferromagnetic ordering for $Ba_3GdRu_2O_9$ is 17.5 J mol^{-1} K^{-1}

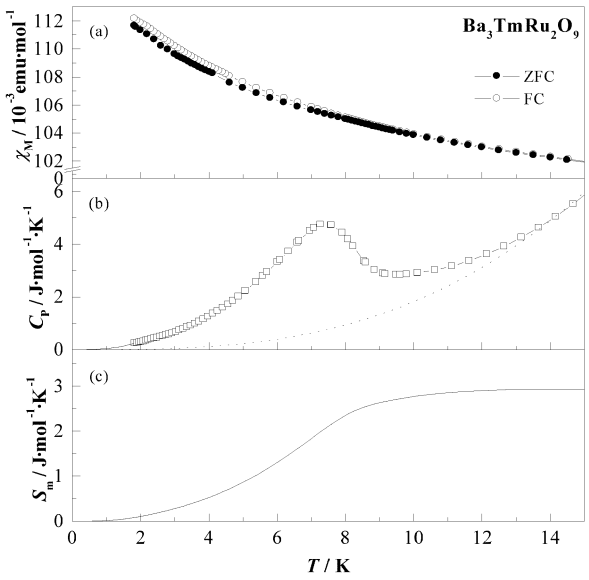

Fig. 7 Temperature dependence of (a) the magnetic susceptibility, (b) the specific heat and (c) the magnetic entropy of $Ba_3TmRu_2O_9$.

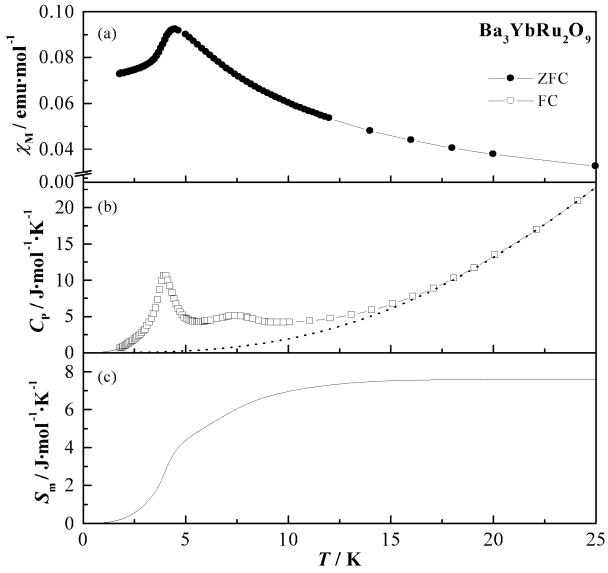

Fig. 8 Temperature dependence of (a) the magnetic susceptibility, (b) the specific heat and (c) the magnetic entropy of $Ba_3YbRu_2O_9$.

(Fig. 4); this value is close to $R \ln W = R \ln 8 = 17.3$ J mol^{-1} K^{-1} (R: molar gas constant, W: number of states for Ln^{3+} ion). This result is consistent with the fact that the ground state for Gd^{3+} ion is $^8S_{7/2}$ (the degeneracy of which is $W = 2S + 1 = 8$) and confirms that the magnetic anomaly at 14.8 K is due to the antiferromagnetic ordering of Gd^{3+} ions.

The magnetic entropy change for $Ba_3HoRu_2O_9$ is 14.7 J mol^{-1} K^{-1} (Fig. 5). In an octahedral crystal field environment, the ground state of $^5I_8$ for the Ho^{3+} ion is a singlet state Γ_1 or a doublet state Γ_3, and there exists a low lying exited state (Γ_4; triplet).[15] If these three states degenerate or if the energy difference among them is very small, the expected entropy change due to the Ho^{3+} antiferromagnetic transition is $R \ln 6 = 14.9$ J mol^{-1} K^{-1}. On the other hand, if the energy difference between Γ_3 and Γ_4 is small and the energy difference between Γ_3 and Γ_1 is large, the expected entropy change is $R \ln 5 = 13.4$ J mol^{-1} K^{-1}. In this case, the excess entropy change may be due to the magnetic ordering of $Ru^{4.5+}{}_2O_9$ dimers.

The magnetic entropy change for $Ba_3ErRu_2O_9$ is 13.0 J mol^{-1} K^{-1} (Fig. 6). The ground state of $^4I_{15/2}$ for the Er^{3+} ion is a quartet state Γ_8 or a doublet state Γ_7 in an octahedral crystal field.[15] In the case that the ground state is Γ_8, the expected entropy change due to the Er^{3+} antiferromagnetic transition, $R \ln 4 = 11.5$ J mol^{-1} K^{-1}, is close to the observed value. The excess entropy change may be due to the magnetic ordering of $Ru^{4.5+}{}_2O_9$ dimers.

The magnetic entropy change for $Ba_3TmRu_2O_9$ is 2.9 J mol^{-1} K^{-1} (Fig. 7). The ground state of $^3H_6$ for the Tm^{3+} ion in $Ba_3TmRu_2O_9$ is a singlet (*i.e.*, Γ_1 or Γ_2).[15] The observed small entropy change should be due to the magnetic ordering of $Ru^{4.5+}{}_2O_9$ dimers.

The magnetic entropy change for $Ba_3YbRu_2O_9$ is 7.6 J mol^{-1} K^{-1} (Fig. 8). In an octahedral crystal environment, the ground state of the Yb^{3+} ion (the state $^2F_{7/2}$) is the Γ_6 doublet; the expected entropy change due to the Yb^{3+} antiferromagnetic transition is $R \ln 2 = 5.8$ J mol^{-1} K^{-1}. We consider that the excess entropy change (1.8 J mol^{-1} K^{-1}) is due to the magnetic ordering of $Ru^{4.5+}{}_2O_9$ dimers. Another small anomaly observed at 7.5 K may be understandable by the same reason.

Summary

The 6H-perovskites $Ba_3LnRu_2O_9$ (Ln = Gd, Ho–Yb) have been synthesized. The Rietveld analyses of their XRD data indicate that the average valency of the Ru ions is +4.5. From their magnetic susceptibility and specific heat measurements, we have found that these compounds show magnetic anomalies at 4–15 K. The estimated magnetic entropy changes associated with these anomalies were explained mainly by the antiferromagnetic ordering of Ln^{3+} ions. Further investigations using other methods such as neutron diffraction measurements are needed to elucidate their magnetic behavior.

Acknowledgement

One of the authors (Y. D.) thanks the Research Fellowships of the Japan Society for the Promotion Science for Young Scientists. This study was supported by the Suhara Memorial Foundation.

References

1 A. Callaghan, C. W. Moeller and R. Ward, *Inorg. Chem.*, 1966, **5**, 1572.
2 Y. Maeno, H. Hashimoto, K. Yoshida, S. Nishizaki, T. Fujita, J. G. Bednorz and F. Lichtenberg, *Nature*, 1994, **372**, 532.
3 Y. Doi and Y. Hinatsu, *J. Phys.: Condens. Matter*, 1999, **11**, 4813.
4 R. D. Burbank and H. T. Evans, *Acta Crystallogr.*, 1948, **1**, 330.
5 Y. Doi, Y. Hinatsu, Y. Shimojo and Y. Ishii, *J. Solid State Chem.*, 2001, **161**, 113.
6 Y. Doi, M. Wakeshima, Y. Hinatsu, A. Tobo, K. Ohoyama and Y. Yamaguchi, *J. Mater. Chem.*, 2001, **11**, 3135.
7 F. Izumi and T. Ikeda, *Mater. Sci. Forum*, 2000, **321–324**, 198.
8 U. Treiber, S. Kemmler-Sack, A. Ehmann, H.-U. Schaller, E. Dürrschmidt, I. Thumm and H. Bader, *Z. Anorg. Allg. Chem.*, 1981, **481**, 143.
9 M. Rath and Hk. Müller-Buschbaum, *J. Alloys Compd.*, 1994, **210**, 119.
10 H. Müller-Buschbaum and B. Mertens, *Z. Naturforsch.*, 1996, **51b**, 79.
11 P. Lightfoot and P. D. Battle, *J. Solid State Chem.*, 1990, **89**, 174.
12 J. Darriet, M. Drillon, G. Villeneuve and P. Hagenmuller, *J. Solid State Chem.*, 1976, **19**, 213.
13 J. Darriet, J. L. Soubeyroux and A. P. Murani, *J. Phys. Chem. Solids*, 1983, **44**, 269.
14 Y. Doi, K. Matsuhira and Y. Hinatsu, *J. Solid State Chem.*, in press.
15 K. R. Lea, M. J. M. Leask and W. P. Wolf, *J. Phys. Chem. Solids*, 1962, **23**, 1381.